Pergamon

Int. J. Heat Mass Transfer. Vol. 39, No. 14, pp. 2977–2987, 1996

0017-9310/96 $15.00+0.00

0017-9310(95)00377-0

Second-moment closure for turbulent scalar transport at various Prandtl numbers

NAOKI SHIKAZONO† and NOBUHIDE KASAGI

Department of Mechanical Engineering, The University of Tokyo, Hongo 7-3-1, Bunkyo-ku, Tokyo 113, Japan

(*Received* 5 *January* 1995 *and in final form* 14 *September* 1995)

Abstract—A new second-moment closure model for turbulent scalar transport is proposed on the basis of the correlation coefficients between the flow variables and their derivatives that appear in the scalar-pressure gradient and dissipation terms of a turbulent scalar flux. Since these correlation coefficients should respond sensitively to a change in any of the time scales characteristic of turbulent transport, the model is given as a function of their ratios, which can be written in terms of turbulent Reynolds number, ($Re_t = k^2/\nu\varepsilon$), Prandtl number ($Pr = \nu/\alpha$) and time scale ratio ($R = (k_\theta/\varepsilon_\theta)/(k/\varepsilon)$). The conventional modeling methodology, i.e. the high Reynolds number hypothesis is abandoned, although the proposed model asymptotes to the well-established model expression in high Reynolds/Peclet number flows. As a result, the scalar fluxes are predicted very well in the homogeneous as well as wall-shear flows over a wide Prandtl number range. Copyright © 1996 Elsevier Science Ltd

1. INTRODUCTION

A mathematical model of turbulent scalar transport is required for solving the Reynolds-averaged scalar equation. With the recent advances in computers, the popularity of second-moment closure, at least in the research community, has considerably increased, though the turbulent Prandtl number models are still in wide use in engineering applications. In the second-moment closure, the generation terms due to mean velocity and scalar gradients can be handled exactly, and this feature should be one of the most attractive advantages when predicting complex flows. In recent years, various mathematical and/or physical constraints such as rapid distortion theory [1], realizability [2] and frame indifference [3] have been taken into account in modeling each of the generating and destruction processes in order to obtain a model of wide applicability; this can only be done for the model of this level. Current efforts are directed toward developing new models, especially of the pressure–scalar gradient correlation term to improve the overall accuracy of existing models [4, 5]. Although the developed models demonstrated improvements in thin shear flows, they sometimes gave poor predictions compared to those obtained by the previous models in more general cases [6, 7]. Besides, an introduction of such additional constraints as those mentioned above has resulted in very complex model structures, which may not be desirable for engineering calculations. There has been even an attempt to intentionally abandon some of the constraints in order to possess a simpler and well-balanced model expression [8].

In scalar flux modeling, the major weakness lies in the fact that most of the scalar field models are developed in the same modeling procedure as the velocity field models. Therefore, they are basically applicable only for gaseous flows at $Pr \approx 1$ and their physical basis is questionable when the Prandtl number is far from unity. For predicting various Prandtl number fluid flows, several turbulent Prandtl number models [9–11] and scalar field two-equation models [12] can be found in the literature, but only a few second-moment closures have been proposed so far [13, 14]. A difficulty exists in the choice of the relevant time scales that are indispensable to modeling unknown correlations between velocity and scalar fluctuations. For instance, even for a simple scalar field, it is not physically clear which time scale, k/ε or $k_\theta/\varepsilon_\theta$, should be adopted, and the selection will be even more ambiguous in low Peclet number flows with additional time scales such as $\sqrt{(\alpha/\varepsilon)}$. It is impossible, however, to incorporate these effects into the model only from a dimensional argument. Hence, a new approach must be introduced. Furthermore, it is known that the scalar–pressure gradient correlation term is not generally aligned with either the scalar flux vector or the mean scalar gradient vector; one can expect a serious difficulty in deriving a simple relationship among these vectors. This is actually the case in strongly sheared turbulence, where the ratio of the streamwise to cross-stream scalar flux components is considerably large ($-\overline{u_1\theta}/\overline{u_2\theta} > 2$), whereas that of the scalar–pressure gradient correlation term remains moderate [5, 15].

From the viewpoints above, we presently construct

† Present address: Mechanical Engineering Research Laboratory, Hitachi, Ltd, 502 Kandatsu, Tsuchiura, Ibaraki 300, Japan.

NOMENCLATURE

- a_{ij} stress anisotropy, $\overline{u_iu_j}/k-2/3\delta_{ij}$
- A flatness parameter, $1-9/8(A_2-A_3)$
- A_2 second invariant of stress anisotropy, $a_{ij}a_{ij}$
- A_3 third invariant of stress anisotropy, $a_{ij}a_{jk}a_{ki}$
- $f_{\varepsilon 1}, f_{\varepsilon 2}$ functions in $\varepsilon_{i\theta}$ model, equation (12)
- $f_{\Pi 1}, f_{\Pi 2}$ functions in $\Pi_{i\theta}$ model, equation (11)
- f_w weighting function in the near-wall region, equations (50), (51) and (52)
- k turbulent kinetic energy, $\overline{u_iu_i}/2$
- k_θ scalar variance, $\overline{\theta^2}/2$
- Nu Nusselt number
- P production of turbulent kinetic energy
- Pr Prandtl number, ν/α
- Pr_t turbulent Prandtl number
- $P_{i\theta}$, P_θ production terms of turbulent scalar flux and scalar variance, in equations (1) and (37)
- R time scale ratio, $(k_\theta/\varepsilon_\theta)/(k/\varepsilon)$
- Re_t turbulent Reynolds number, $k^2/\nu\varepsilon$
- S mean velocity gradient, $\partial U_1/\partial x_2$
- t time
- $T_{i\theta}$, T_θ, $T_{\varepsilon\theta}$ turbulent diffusion terms of turbulent scalar flux, scalar variance and its dissipation rate, in equations (1), (37) and (39)
- U_i, u_i mean and fluctuating velocity components
- $V_{i\theta}$ molecular diffusion term of turbulent scalar flux, in equation (1)
- x_i ith coordinate.

Greek symbols

- α thermal diffusivity
- ε, ε_θ dissipation terms of k and k_θ
- $\varepsilon_{i\theta}$ dissipation term of turbulent scalar flux, in equation (1)
- Θ, θ mean and fluctuating scalar
- λ Taylor microscale, $\sqrt{(10\nu k/\varepsilon)}$
- λ_θ scalar Taylor microscale, $\sqrt{(12\alpha k_\theta/\varepsilon_\theta)}$
- ν kinematic viscosity
- $\Pi_{i\theta}$ scalar-pressure gradient correlation term, in equation (1)
- ρ density
- $\phi_{i\theta}$ pressure-scalar gradient correlation term, in equation (2).

Subscripts and superscripts

- $()_{,i}$ partial derivative with respect to x_i
- $\overline{()}$ ensemble average
- $()'$ root-mean-square value.

a second-moment closure that can be applied to flows of a wide Reynolds and Prandtl number range. In other words, the dependence of the model on the turbulent Reynolds number Re_t, the molecular Prandtl number Pr and the time scale ratio R is properly accounted for. This cannot be done from a dimensional analysis alone, and in the present study, we pay special attention to the correlation coefficients between unknown variables, since they are greatly affected by the parameters mentioned above [16].

The following section describes the derivation of a second closure for handling multiple time scale problem of turbulence. Then, the model is tested and evaluated in several homogeneous flows and in fully-developed channel flows at various Prandtl and Reynolds numbers.

2. MODEL DEVELOPMENT

2.1. *Modeling* $\Pi_{i\theta}$ *and* $\varepsilon_{i\theta}$

When any buoyancy effect can be neglected, the transport equation for the scalar flux in a fluid of constant physical properties is given as:

$$\frac{D\overline{u_i\theta}}{Dt} = \underbrace{-\overline{u_iu_k}\frac{\partial\Theta}{\partial x_k} - \overline{u_k\theta}\frac{\partial U_i}{\partial x_k}}_{P_{i\theta}} \underbrace{-\frac{1}{\rho}\overline{\theta\frac{\partial p}{\partial x_i}}}_{\Pi_{i\theta}} \underbrace{-(\alpha+\nu)\overline{\frac{\partial\theta}{\partial x_k}\frac{\partial u_i}{\partial x_k}}}_{\varepsilon_{i\theta}} \underbrace{-\frac{\partial}{\partial x_k}\overline{u_iu_k\theta}}_{T_{i\theta}} + \underbrace{\frac{\partial}{\partial x_k}\left(\alpha\overline{u_i\frac{\partial\theta}{\partial x_k}}+\nu\overline{\theta\frac{\partial u_i}{\partial x_k}}\right)}_{V_{i\theta}}. \quad (1)$$

The scalar–pressure gradient correlation term $\Pi_{i\theta}$ and the dissipation term $\varepsilon_{i\theta}$ are major sink terms and need to be carefully modeled. In conventional turbulence modeling, $\Pi_{i\theta}$ has been divided into the pressure–scalar gradient correlation term $\phi_{i\theta}$ and the pressure diffusion term; the latter has been usually ignored or thought of as being absorbed into the turbulent diffusion term:

$$\underbrace{-\frac{1}{\rho}\overline{\theta\frac{\partial p}{\partial x_i}}}_{\Pi_{i\theta}} = \underbrace{\frac{1}{\rho}\overline{p\frac{\partial\theta}{\partial x_i}}}_{\phi_{i\theta}} \underbrace{-\frac{1}{\rho}\frac{\partial\overline{p\theta}}{\partial x_i}}_{\text{pressure diff.}}. \quad (2)$$

The dissipation term has been assumed to be isotropic ($\varepsilon_{i\theta} = 0$) and the effect of anisotropic dissipation has been expressed implicity within the model of $\phi_{i\theta}$. This reduces the problem to the modeling of $\phi_{i\theta}$ alone, and one of the simplest model for $\phi_{i\theta}$ is written as [17] (Basic model, hereafter):

$$\phi_{i\theta} = -3.0\frac{\varepsilon}{k}\overline{u_i\theta}+0.5\overline{u_k\theta}\frac{\partial U_i}{\partial x_k}. \tag{3}$$

However, there are some situations where this approach seems inappropriate, e.g. in low Peclet number flows $\varepsilon_{i\theta}$ dominates the flux destruction mechanism. Since $\Pi_{i\theta}$ and $\varepsilon_{i\theta}$ represent physically distinct mechanisms, they are modeled separately in this study.

We define the correlation coefficients of $\Pi_{i\theta}$ and $\varepsilon_{i\theta}$, respectively, as follows:

$$-\frac{1}{\rho}\overline{\theta\frac{\partial p}{\partial x_i}}\bigg/\left[\frac{1}{\rho}\sqrt{(\overline{\theta^2})}\sqrt{\left(\overline{\left(\frac{\partial p}{\partial x_{(i)}}\right)^2}\right)}\right] \tag{4}$$

$$(\nu+\alpha)\overline{\frac{\partial u_i}{\partial x_j}\frac{\partial \theta}{\partial x_j}}\bigg/\left[(\nu+\alpha)\sqrt{\left(\overline{\left(\frac{\partial u_{(i)}}{\partial x_k}\right)^2}\right)}\sqrt{\left(\overline{\left(\frac{\partial \theta}{\partial x_l}\right)^2}\right)}\right] \tag{5}$$

where the indices in parentheses do not obey the summation convention rule. If the two fluctuating components, i.e. θ and $\partial p/\partial x_i$, or $\partial u_i/\partial x_k$ and $\partial\theta/\partial x_k$, are well correlated, the above coefficients should be of the order of one. However, the correlations between those components are generally poor, because they are associated with different scales. For example, fluctuations such as u and θ are tuned to low wave numbers, whereas $\partial p/\partial x_i$, $\partial u_i/\partial x_j$ and $\partial\theta/\partial x_i$ are the spacial derivatives of fluctuating quantities that become large at high wave numbers. With these facts, the modeling of $\Pi_{i\theta}$ and $\varepsilon_{i\theta}$ should be especially difficult. For example, the correlation between velocity–scalar fluctuations at low wave numbers and scalar–velocity fluctuations at high wave numbers is hard to parameterize. Besides, when Prandtl number is apart from unity, the velocity and scalar scales characteristic of high wave numbers become much different, because viscous and molecular diffusivities affect the velocity and scalar fields differently.

In this study, we assume that dimensionless form of $\Pi_{i\theta}$ can be generally related to functions of the scalar flux and its production terms as:

$$\frac{-\frac{1}{\rho}\overline{\theta\frac{\partial p}{\partial x_i}}}{\frac{1}{\rho}\sqrt{(\overline{\theta^2})}\sqrt{\left(\overline{\left(\frac{\partial p}{\partial x_{(i)}}\right)^2}\right)}} = \text{func.}\left(\frac{\overline{u_i\theta}}{\sqrt{(\overline{u_{(i)}^2})}\sqrt{(\overline{\theta^2})}},\ \frac{-\overline{u_iu_j}\frac{\partial \Theta}{\partial x_j}}{P\sqrt{(k_\theta/k)}},\ \frac{-\overline{u_j\theta}\frac{\partial U_i}{\partial x_k}}{P\sqrt{(k_\theta/k)}},\ldots\right). \tag{6}$$

Since the above equation simply shows the relation between the anisotropy of dimensionless variables, we retain only the correlation coefficient of the scalar flux in the right-hand side of equation (6) for the first-order approximation. The effect of mean velocity gradient on fluctuating pressure will be expressed implicitly through P/ε in the model of $\sqrt{(\overline{p^2})}$ [see equation (28)]. If we further assume that the correlation coefficient of $\varepsilon_{i\theta}$ should be also a function of that of the scalar flux, we have:

$$\frac{\Pi_{i\theta}}{\frac{1}{\rho}\sqrt{(\overline{\theta^2})}\sqrt{\left(\overline{\left(\frac{\partial p}{\partial x_{(i)}}\right)^2}\right)}} = C_\Pi f_{\Pi 1} f_{\Pi 2}\frac{\overline{u_i\theta}}{\sqrt{(\overline{u_{(i)}^2})}\sqrt{(\overline{\theta^2})}} \tag{7}$$

$$\frac{\varepsilon_{i\theta}}{(\nu+\alpha)\sqrt{\left(\overline{\left(\frac{\partial u_{(i)}}{\partial x_k}\right)^2}\right)}\sqrt{\left(\overline{\left(\frac{\partial \theta}{\partial x_l}\right)^2}\right)}} = C_\varepsilon f_{\varepsilon 1} f_{\varepsilon 2}\frac{\overline{u_i\theta}}{\sqrt{(\overline{u_{(i)}^2})}\sqrt{(\overline{\theta^2})}} \tag{8}$$

where

$$0 \leqslant f_{\Pi 1}, f_{\Pi 2}, f_{\varepsilon 1}, f_{\varepsilon 2} \leqslant 1.$$

Note that the coefficients C_Π and C_ε should be of O(1) and that the functions $f_{\Pi 1}, f_{\Pi 2}, f_{\varepsilon 1}$ and $f_{\varepsilon 1}$ and $f_{\varepsilon 2}$ vary from unity to zero in order to express the decrease in the correlation coefficients of $\Pi_{i\theta}$ and $\varepsilon_{i\theta}$. Functions $f_{\Pi 1}$ and $f_{\varepsilon 1}$ stand for the effect of scale difference between large and fine motions. On the other hand, functions $f_{\Pi 2}$ and $f_{\varepsilon 2}$ represent the effect of scale difference between scalar and velocity fluctuations at high wave numbers. Note that each side of these equations will not take a value much far from unity, but this constraint has not been taken into account in the previous models.

Equations (7) and (8) contain variables such as the derivative of fluctuating pressure, which should require further modeling. The pressure fluctuation is related to the turbulent kinetic energy as $\sqrt{(\overline{p^2})} = C_p\rho k$. For the pressure derivative tensor $\overline{p_{,i}p_{,j}}$, the following two candidate expressions are adopted as a first-order approximation:

$$\frac{1}{\rho^2}\overline{\frac{\partial p}{\partial x_i}\frac{\partial p}{\partial x_j}} \sim \frac{1}{3}\frac{1}{\rho^2}\overline{\frac{\partial p}{\partial x_k}\frac{\partial p}{\partial x_k}}\delta_{ij} \sim C_p^2\frac{k^2}{\lambda^2}\delta_{ij} \tag{9}$$

$$\frac{1}{\rho^2}\overline{\frac{\partial p}{\partial x_i}\frac{\partial p}{\partial x_j}} \sim \frac{1}{\rho^2}\overline{\frac{\partial p}{\partial x_k}\frac{\partial p}{\partial x_k}}\frac{\overline{u_iu_j}}{2k} \sim C_p^2\frac{k^2}{\lambda^2}\frac{\overline{u_iu_j}}{k} \tag{10}$$

where λ is the Taylor microscale. With these estimates introduced into equation (7), we have two general models for the scalar-pressure gradient correlation term as:

$$\Pi_{i\theta} = \begin{cases} C_\Pi f_{\Pi 1} f_{\Pi 2} C_p \sqrt{(Re_t)} \sqrt{\left(\frac{k}{2\overline{u_{(i)}^2}}\right)} \frac{\varepsilon}{k} \overline{u_i\theta} & \text{(Model 1)} \\ \frac{\sqrt{3}}{2} C_\Pi f_{\Pi 1} f_{\Pi 2} C_p \sqrt{(Re_t)} \frac{\varepsilon}{k} \overline{u_i\theta} & \text{(Model 2).} \end{cases} \tag{11}$$

The coefficient $\sqrt{(3)}/2$ is introduced so that Models 1 and 2 give exactly the same form in isotropic turbulence. If we also assume $\nu\overline{u_{i,k}u_{j,k}}/\varepsilon = \overline{u_i u_j}/2k$ in low Reynolds number flows, where $\varepsilon_{i\theta}$ is important, equation (8) can be rewritten as:

$$\varepsilon_{i\theta} = C_\varepsilon f_{\varepsilon 1} f_{\varepsilon 2} \frac{1+Pr}{2\sqrt{(Pr)}\sqrt{(R)}} \frac{\varepsilon}{k} \overline{u_i\theta}. \tag{12}$$

These equations do not satisfy some modeling constraints, i.e. vectorial invariance (Model 1), realizability [18] and linear property of scalar equations [19]. In the following, each of the model functions $f_{\Pi 1}$, $f_{\Pi 2}$, $f_{\varepsilon 1}$ and $f_{\varepsilon 2}$ is determined.

As mentioned earlier, the scalar-pressure gradient correlation term $\Pi_{i\theta}$ can be written as a sum of the pressure–scalar gradient correlation term $\phi_{i\theta}$ and the pressure diffusion term. In most practical flows and far from a wall, the pressure diffusion term is relatively small, and the following relation should be a good approximation:

$$\underbrace{-\frac{1}{\rho}\overline{\theta\frac{\partial p}{\partial x_i}}}_{\Pi_{i\theta}} = \underbrace{\frac{1}{\rho}\overline{p\frac{\partial \theta}{\partial x_i}}}_{\phi_{i\theta}}. \tag{13}$$

Through the same modeling procedure for $\Pi_{i\theta}$, a model of $\phi_{i\theta}$ can also be obtained as:

$$\phi_{i\theta} = \begin{cases} C_\phi f_{\phi 1} f_{\phi 2} C_p \sqrt{(Re_t)} \frac{\sqrt{(Pr)}}{\sqrt{(R)}} \sqrt{\left(\frac{k}{2\overline{u_{(i)}^2}}\right)} \frac{\varepsilon}{k} \overline{u_i\theta} \\ \text{(Model 1)} \\ \frac{\sqrt{3}}{2} C_\phi f_{\phi 1} f_{\phi 2} C_p \sqrt{(Re_t)} \frac{\sqrt{(Pr)}}{\sqrt{(R)}} \frac{\varepsilon}{k} \overline{u_i\theta} \\ \text{(Model 2)} \end{cases} \tag{14}$$

where a relationship $\sqrt{(\overline{(\partial\theta/\partial x_i)^2})} = \sqrt{(\varepsilon_\theta/\alpha)}$ is utilized. The difference between equations (11) and (14) originates from the choice of the length scales that are used for estimating the derivatives of fluctuation quantities, i.e. $\lambda/\lambda_\theta \propto \sqrt{(Pr/R)}$ (λ_θ is the Taylor microscale of scalar fluctuations). Therefore, if the spectra of turbulent energy and scalar variance do not overlap at a high wave-number range ($\lambda \neq \lambda_\theta$), and also if the functions $f_{\Pi 2}$ and $f_{\phi 2}$ are of order one, equations (11) and (14) may give greatly different results. In order for the model to satisfy the condition of (13), the correlation coefficients of $\Pi_{i\theta}$ and $\phi_{i\theta}$ must decrease accordingly. Thus $f_{\Pi 2}$ and $f_{\phi 2}$ must satisfy at least the following inequalities:

$$f_{\Pi 2} \leqslant \min\left[1, \frac{C_\phi}{C_\Pi}\frac{\sqrt{(Pr)}}{\sqrt{(R)}}\right] \tag{15}$$

$$f_{\phi 2} \leqslant \min\left[1, \frac{C_\Pi}{C_\phi}\frac{\sqrt{(R)}}{\sqrt{(Pr)}}\right]. \tag{16}$$

The physical meaning of these inequalities is that the derivative of a fluctuating quantity which appears in the correlation should be estimated at least at a scale larger than both λ and λ_θ ($\partial/\partial x_i \leqslant O$ (min[$1/\lambda$, $1/\lambda_\theta$])). In other words, the derivative of a fluctuating quantity with the length scale smaller than either of λ or λ_θ cannot correlate well with other fluctuations such as θ or p.

We now return to the transport equation of $\overline{u_i\theta}$. If a local equilibrium condition holds, the transport equation of $\overline{u_i\theta}$ can be written as:

$$0 = P_{i\theta} + \Pi_{i\theta} - \varepsilon_{i\theta}. \tag{17}$$

With the assumptions that $\overline{u_i\theta} \sim \sqrt{(kk_\theta)}$, $\overline{u_iu_j} \sim k$, $\partial U_i/\partial x_j \sim \varepsilon/k$ and $\partial\Theta/\partial x_i \sim C_R\varepsilon_\theta/\sqrt{(kk_\theta)}$, the order of magnitude of each term can be estimated as:

$$P_{i\theta} = O\left(\frac{\varepsilon}{k}\sqrt{(kk_\theta)}\left[\frac{C_R}{R}+1\right]\right) \tag{18}$$

$$\Pi_{i\theta} = O\left(\frac{\varepsilon}{k}\sqrt{(kk_\theta)}[\sqrt{(Re_t)} f_{\Pi 1} f_{\Pi 2}]\right) \tag{19}$$

$$\varepsilon_{i\theta} = O\left(\frac{\varepsilon}{k}\sqrt{(kk_\theta)}\left[\frac{1+Pr}{\sqrt{(Pr)}\sqrt{(R)}} f_{\varepsilon 1} f_{\varepsilon 2}\right]\right). \tag{20}$$

In order to restrict $\Pi_{i\theta}$ and $\varepsilon_{i\theta}$ not to exceed $P_{i\theta}$, the following inequalities must be satisfied:

$$\sqrt{(Re_t)} f_{\Pi 1} f_{\Pi 2} \leqslant c'\left(\frac{C_R}{R}+1\right) \tag{21}$$

$$\frac{1+Pr}{\sqrt{(Pr)}\sqrt{(R)}} f_{\varepsilon 1} f_{\varepsilon 2} \leqslant c''\left(\frac{C_R}{R}+1\right). \tag{22}$$

The coefficients c' and c'' should be of $O(1)$. The functions $f_{\Pi 1}$, $f_{\Pi 2}$, $f_{\varepsilon 1}$ and $f_{\varepsilon 2}$ are now chosen so that relationships of (15), (21) and (22) should hold at any state, e.g. $Pr \to 0$ or ∞, and $Re_t \to 0$ or ∞. As mentioned earlier, functions $f_{\Pi 1}$ and $f_{\varepsilon 1}$ are chosen so as to express the effect of broadening of the spectra, while functions $f_{\Pi 2}$ and $f_{\varepsilon 2}$ must bear the effect of scale difference between scalar and velocity fields at high wave numbers. Finally, these functions are modeled as follows:

$$f_{\Pi 1} = 1 - \exp(-10r) \tag{23}$$

$$f_{\varepsilon 1} = 1 - \exp(-10r) \tag{24}$$

$$f_{\Pi 2} = \min\left[1, \frac{1}{1.2}\frac{\sqrt{(Pr)}}{\sqrt{(R)}}\right] \tag{25}$$

$$f_{\varepsilon 2} = \min\left[6\frac{\sqrt{(Pr)}}{\sqrt{(R)}}, 1, \frac{\sqrt{(R)}}{\sqrt{(Pr)}}\right] \tag{26}$$

where $r = (C_R/R+1)/(\sqrt{(Re_t)}f_{\Pi 2})$. The constants in equations (23)–(26) are optimized by referring to the direct numerical simulation (DNS) and experimental results satisfactorily. It must be noted that, since function $f_{\varepsilon 1}$ cannot be determined only from the condition of (22), it is assumed equal to $f_{\Pi 1}$ in order to conform to a locally isotropic state, i.e. $\varepsilon_{i\theta} \to 0$ if $r \to 0$.

The parameter $\sqrt{(Pr/P)}$ that appears in $f_{\Pi 2}$ and $f_{\varepsilon 2}$ is the ratio between the Taylor microscales of velocity and scalar fluctuations, λ and λ_θ. It can also be considered as the time scale ratio between the velocity and scalar fields at high wave-number regions, when the same velocity scale is used for conversion from length to time scales. On the other hand, the parameter r in $f_{\Pi 1}$ and $f_{\varepsilon 1}$ can be interpreted as the ratio of the two characteristic time scales, if rewriting it as:

$$r = \frac{\max\left[\sqrt{\left(\frac{\nu}{\varepsilon}\right)}\, 1.2\sqrt{\left(\frac{\nu}{\varepsilon}\right)}\sqrt{\left(\frac{R}{Pr}\right)}\right]}{1\bigg/\left(\frac{1}{k/\varepsilon}+\frac{C_R}{k_\theta/\varepsilon_\theta}\right)}. \quad (27)$$

The numerator denotes the choice of the larger between the two fine time scales, while the denominator the smaller between the two large time scales. Thus, the rates of decrease of the correlation coefficients are proportional to these time and length scale ratios, $\sqrt{(Pr/R)}$ and r. With equations (23)–(26), the proper characteristic time scales are automatically selected when the present model is applied to a flow which involves time scales.

As previously noted, the coefficient C_p relates the pressure fluctuation to the turbulent kinetic energy k. Since we didn't deal so far the so-called slow and rapid parts of $\Pi_{i\theta}$ separately, C_p must represent the effects of these processes. For example, the DNS data [20] show that C_p takes a larger value in the presence of mean velocity gradient, while it decreases remarkably near a wall since $\sqrt{(\overline{p^2})}$ does not show a strong peak as k. In order to account for these features, C_p is expressed as a function of P/ε and the flatness parameter A as:

$$C_p = \sqrt{(A)}\left(0.8+0.3\frac{P}{\varepsilon}\right) \quad (28)$$

where $A = 1-9/8(a_{ij}a_{ij}-a_{ij}a_{jk}a_{ki})$, $a_{ij} = (\overline{u_iu_j}/k-2/3\delta_{ij})$ and $P = -\overline{u_iu_j}\,\partial U_i/\partial x_j$.

An *a priori* test of equations (11) and (12) with the aid of DNS and experimental data in several fundamental flows is described below. Here, the sum of scalar-pressure gradient correlation and dissipation terms is compared with:

$$\Pi_{1\theta}-\varepsilon_{1\theta} = -C_{(1)}\frac{\varepsilon}{k}\overline{u_1\theta} \quad (29)$$

$$\Pi_{2\tau}-\varepsilon_{2\theta} = -C_{(2)}\frac{\varepsilon}{k}\overline{u_2\theta} \quad (30)$$

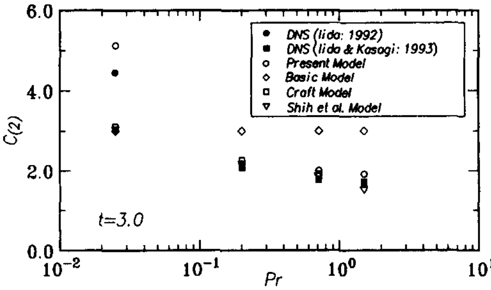

Fig. 1. Dependence of the model constant of $\Pi_{i\theta}-\varepsilon_{i\theta}$ on the Prandtl number in isotropic turbulence with a constant mean scalar gradient.

$$\Pi_{3\theta}-\varepsilon_{3\theta} = -C_{(3)}\frac{\varepsilon}{k}\overline{u_3\theta} \quad (31)$$

where the model constant $C_{(i)}$ is given by the present model as follows:

$$C_{(i)} = 0.264 f_{\Pi 1}f_{\Pi 2}\sqrt{(A)}\left(0.8+0.3\frac{P}{\varepsilon}\right)\sqrt{(Re_t)}\sqrt{\left(\frac{k}{2\overline{u_{(i)}^2}}\right)} + 0.8 f_{\varepsilon 1}f_{\varepsilon 2}\frac{1+Pr}{2\sqrt{(Pr)}\sqrt{(R)}} \quad \text{(Model 1)} \quad (32)$$

$$C_{(i)} = 0.264\frac{\sqrt{3}}{2} f_{\Pi 1}f_{\Pi 2}\sqrt{(A)}\left(0.8+0.3\frac{P}{\varepsilon}\right)\sqrt{(Re_t)} + 0.8 f_{\varepsilon 1}f_{\varepsilon 2}\frac{1+Pr}{2\sqrt{(Pr)}\sqrt{R)}} \quad \text{(Model 2)}. \quad (33)$$

The DNS or experimental data are directly substituted into the model expression [equations (32) and (33)] and compared with the results obtained from the definition [$\Pi_{i\theta}$ and $\varepsilon_{i\theta}$, in equations (29)–(31)].

First, the model is tested in isotropic turbulence with a constant mean scalar gradient ($\partial\Theta/\partial x_2 =$ const.). In isotropic turbulence, $C_{(i)}$ corresponds to the model constant of the slow term. Note that both Models 1 and 2 take exactly the same form in this flow. In Fig. 1, the Prandtl number dependence of $C_{(2)}$ is shown. The predictions of Craft [5] and Shih *et al.* [21] are also included for comparison. The DNS data [22, 23] reveal that the value of this constant increase in low Pr and asymptotes to a value around 1.7 at high Pr. This tendency is well captured by the present model. The effect of the turbulent Reynolds number is shown in Fig. 2. The value of $C_{(2)}$ increases with Re_t as indicated by the experimental data of Maekawa and Kobayashi [24]. In their experiment, the ratio of the grid diameter d to the mesh size M is changed in order to produce four different Reynolds number flows; e.g. $Re_t^{\text{init}} \approx 100$ for $d/M = 0.15$ and $Re_t^{\text{init}} \approx 330$ for $d/M = 0.30$. This Reynolds number dependence is predicted only by the present model. Finally, the effect of time scale ratio is shown in Fig. 3. The experimental data of Sirivat and Warhaft [25] show that $C_{(2)}$ slightly decreases as R increases. Note that the closed symbols denote experiments performed

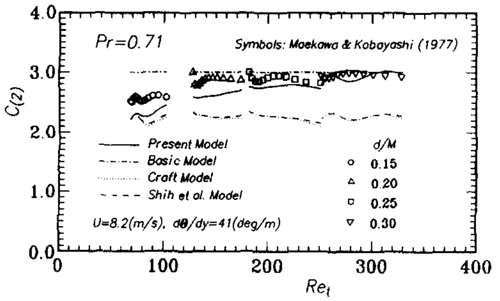

Fig. 2. Dependence of the model constant of $\Pi_{i\theta}-\varepsilon_{i\theta}$ on the turbulent Reynolds number in isotropic turbulence with a constant mean scalar gradient.

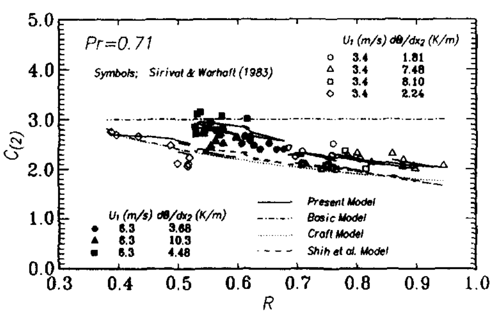

Fig. 3. Dependence of the model constant of $\Pi_{i\theta}-\varepsilon_{i\theta}$ on the time scale ratio in isotropic turbulence with a constant mean scalar gradient.

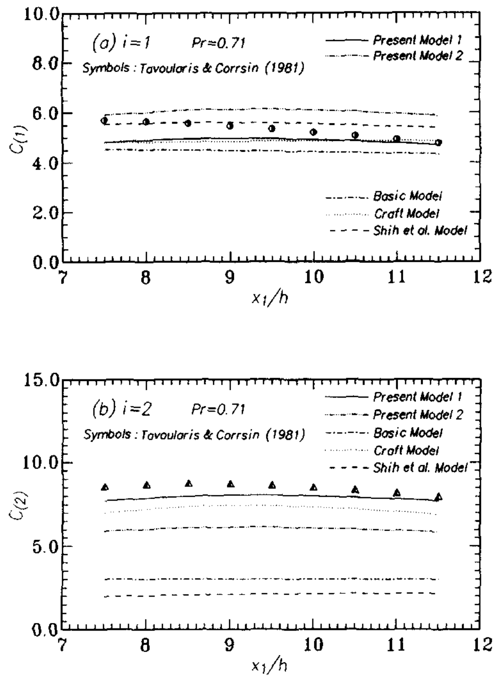

Fig. 4. Dependence of the model constant $\Pi_{i\theta}-\varepsilon_{i\theta}$ on the mean shear rate in homogeneous shear flow with constant mean scalar gradients.

at a slightly higher Reynolds number than the cases denoted by the open symbols. The Reynolds number effect is well predicted again by the present model.

Secondly, the experimental data of homogeneous shear flow [26] is utilized. In this case, $C_{(1)}$ as well as $C_{(2)}$ can be defined. As seen in Fig. 4, the value of $C_{(2)}$ is about 1.7 times larger than that of $C_{(1)}$, and this is the major reason why most of the conventional models fail in this flow. Jones and Musonge [15] and also Craft [5] introduced a term which contains the mean scalar gradient into the modeled pressure–scalar gradient correlation term to overcome this problem. The present Model 1 can also express this strongly anisotropic feature by introducing the correlation coefficient of the turbulent scalar flux as a variable.

2.2. *Modeling* $T_{i\theta}$ *and* $V_{i\theta}$

The generalized gradient diffusion hypothesis (GGDH) is used to model the turbulent diffusion term $T_{i\theta}$:

$$T_{i\theta} = \frac{\partial}{\partial x_k}\left(C_{\theta 1} f_{\mathrm{R}} \frac{k}{\varepsilon}\overline{u_j u_k}\frac{\partial \overline{u_i\theta}}{\partial x_j}\right) \tag{34}$$

where, f_{R} is a function of R which is derived from the eddy diffusivity for a local equilibrium flow as:

$$f_{\mathrm{R}} = \frac{2}{\left(\dfrac{C_{\mathrm{R}}}{R}+1\right)}. \tag{35}$$

This function takes the smaller of k/ε and $k_\theta/\varepsilon_\theta$ as the characteristic time scale that appears in $T_{i\theta}$.

The molecular diffusion term $V_{i\theta}$ also needs to be modeled. In the present study, the following simple model is adopted:

$$V_{i\theta} = \frac{(\nu+\alpha)}{2}\frac{\partial^2 \overline{u_i\theta}}{\partial x_k^2}. \tag{36}$$

2.3. *Modeling* k_θ *and* ε_θ *equations*

In order to calculate the scalar invariance and scalar time scale, the equations of k_θ and ε_θ must be solved. The transport equation of the scalar variance $k_\theta = \overline{\theta^2}/2$ can be written as:

$$\frac{\mathrm{D}k_\theta}{\mathrm{D}t} = \underbrace{\alpha\frac{\partial^2 k_\theta}{\partial x_i^2}}_{V_\theta} \underbrace{-\frac{\partial}{\partial x_i}\overline{u_i\theta^2}}_{T_\theta} \underbrace{-\overline{u_i\theta}\frac{\partial \Theta}{\partial x_i}}_{P_\theta} - \underbrace{\alpha\overline{\frac{\partial\theta}{\partial x_i}\frac{\partial\theta}{\partial x_i}}}_{\varepsilon_\theta}. \tag{37}$$

The turbulent diffusion term T_θ and the dissipation term ε_θ are the unknown terms in equation (37). For T_θ, a GGDH model is adopted:

$$T_\theta = \frac{\partial}{\partial x_k}\left(C_{\theta 2} f_{\mathrm{R}}\frac{k}{\varepsilon}\overline{u_j u_k}\frac{\partial k_\theta}{\partial x_j}\right). \tag{38}$$

The dissipation term ε_θ is given from the following modeled equation:

Table 1. Model constants

C_Π	C_ε	C_R	$C_{\theta 1}, C_{\theta 2}, C_{\theta 3}$	C_{P1}	C_{P2}	C_{D1}	C_{D2}
−0.264	0.8	0.7	0.3	0.8	0.3	1.0	0.3

$$\frac{D\varepsilon_\theta}{Dt} = \alpha \frac{\partial^2 \varepsilon_\theta}{\partial x_i^2} + T_{\varepsilon\theta} + C_{P1}\frac{P_\theta}{k_\theta}\varepsilon_\theta + C_{P2}\frac{P}{k}\varepsilon_\theta - C_{D1}\frac{\varepsilon_\theta}{k_\theta}\varepsilon_\theta - C_{D2}\frac{\varepsilon}{k}\varepsilon_\theta. \quad (39)$$

The turbulent diffusion term $T_{\varepsilon\theta}$ is modeled in the same manner as $T_{i\theta}$ and T_θ:

$$T_{\varepsilon\theta} = \frac{\partial}{\partial x_k}\left(C_{\theta 3} f_R \frac{k}{\varepsilon}\overline{u_j u_k}\frac{\partial \varepsilon_\theta}{\partial x_j}\right). \quad (40)$$

The values of the model constants in the turbulent diffusion terms (34), (38) and (40) are set as $C_{\theta 1} = C_{\theta 2} = C_{\theta 3} = 0.3$, since these values give good results in channel flows. The model constants in equation (39) are optimized so that it gives good results in isotropic turbulence, homogeneous shear and channel flows. The values of the model constants are summarized in Table 1.

3. MODEL TESTING IN BASIC FLOWS

The model described in the previous section is tested in several fundamental flows.† The velocity field variables (i.e. U_i, $\overline{u_i u_j}$ and ε) are supplied from the DNS and experimental data, and the differential equations only for Θ, $\overline{u_i\theta}$, k_θ and ε_θ are solved, so that any failure in the results can be attributed to the scalar field modeling.

3.1. *Homogeneous shear flow*

The DNS of Rogers *et al.* [27] are utilized. In their simulation, the constant mean scalar gradient is imposed in three orthogonal directions; cases 1, 2 and 3 correspond the mean scalar gradient in the x_1, x_2 and x_3 directions, respectively. Most turbulence models have been tested and qualified against the case in which the mean scalar gradient is aligned with the mean velocity gradient. Hence, it is important to study how those models perform in the case when the scalar gradient exists in other directions. The model predictions for the three cases are shown in Fig. 5. The present model and the Basic model give fairly good results in all cases, while other recent complex models achieve poorly, especially in case 1. This implies that the additional terms in the complex models do possess a possibility of giving erroneous results in the case where they have not been tested, while simpler models seem not to fail seriously.

† The results in the flows which were already utilized in the *a priori* test in Section 2 (see Figs 1–4) will not be shown here. However, it is confirmed that the present model gives good results in those flows.

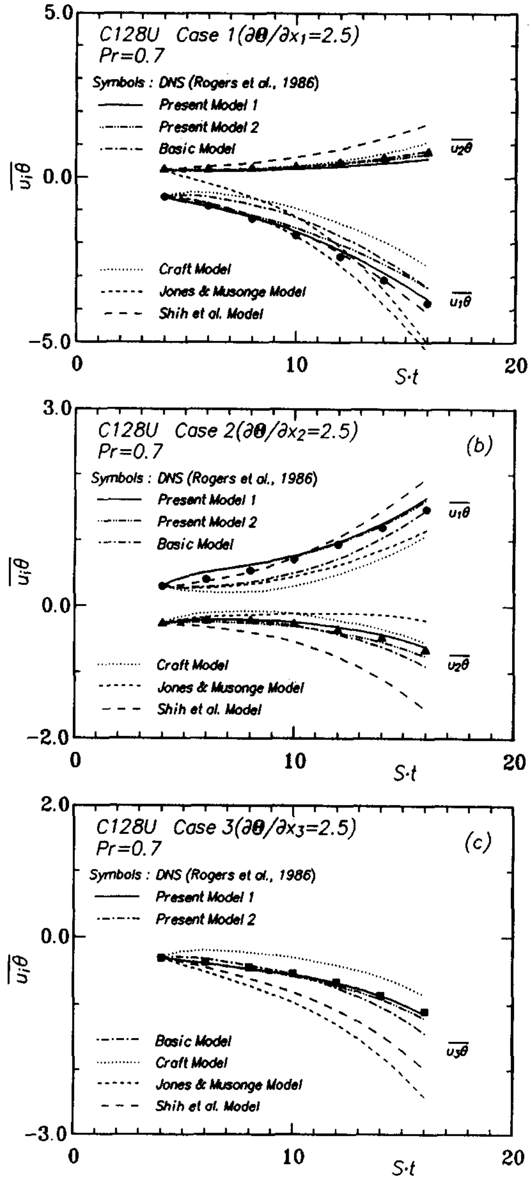

Fig. 5. Time development of turbulent scalar flux in homogeneous shear flow. (a) Case 1 ($\partial\Theta/\partial x_1$ = const.), (b) Case 2 ($\partial\Theta/\partial x_2$ = const.), (c) Case 3 ($\partial\Theta/\partial x_3$ = const.).

3.2. *Fully developed channel flow*

The model proposed should be modified for its application to the near-wall sublayer. To do this, a difficulty exists in the prediction of scalar transfer in high Prandtl number fluids as described in the following.

In the present study, the scalar fluctuation is assumed to be zero at the wall. This assumption is generally valid in an air flow (see Kasagi *et al.* [28]). Then the wall limiting value of R is equal to Pr:

$$R = Pr \quad \text{at} \quad y = 0 \quad (41)$$

where y is the distance from the wall. Also, λ_θ becomes of the same order as λ. The local Reynolds number is effectively small ($r \gg 1$) in this region, and hence all the damping functions can be estimated as $f_{\Pi 1} \sim f_{\Pi 2} \sim f_{\varepsilon 1} \sim f_{\varepsilon 2} \sim 1$. If we now assume that the gradients of mean scalar quantities should scale with λ_θ or λ (i.e. $\partial/\partial x_i \sim 1/\lambda_\theta \sim 1/\lambda$), the order of magnitude of the model terms such as equations (11), (12), (34) and (36) can be estimated as follows:

$$T_{i\theta} = O\left(\frac{\varepsilon}{k}\sqrt{(kk_\theta)}\sqrt{(Re_t)}\right) \quad (42)$$

$$V_{i\theta} = O\left(\frac{\varepsilon}{k}\sqrt{(kk_\theta)}\left[\frac{1}{Pr}+1\right]\right) \quad (43)$$

$$\Pi_{i\theta} = O\left(\frac{\varepsilon}{k}\sqrt{(kk_\theta)}\sqrt{(Re_t)}\right) \quad (44)$$

$$\varepsilon_{i\theta} = O\left(\frac{\varepsilon}{k}\sqrt{(kk_\theta)}\left[\frac{1}{Pr}+1\right]\right). \quad (45)$$

However, in the vicinity of the wall (e.g. $y^+ \leqslant 10$), the order of magnitude of the scalar flux production term $P_{i\theta}$ cannot be estimated as in equation (18) when $Pr \gg 1$. The estimation $\partial U_i/\partial x_j \sim C_S\sqrt{(\varepsilon/\nu)}$ should be used instead of $\partial U_i/\partial x_j \sim \varepsilon/k$ since the viscous dissipation of mean kinetic energy $\nu(\partial U_i/\partial x_j)^2$ is of the same order as ε. Then the order of magnitude of $P_{i\theta}$ can be written as:

$$P_{i\theta} = O\left(\frac{\varepsilon}{k}\sqrt{(kk_\theta)}\left[\frac{C_R}{R}+C_S\sqrt{(Re_t)}\right]\right). \quad (46)$$

If the scalar flux equation is assumed to be at a local equilibrium state, $V_{i\theta}$ and $\varepsilon_{i\theta}$ cannot exceed $P_{i\theta}$. In order to satisfy this condition, functions $f_{\varepsilon w}$ and f_{Vw} are introduced into the models of $V_{i\theta}$ and $\varepsilon_{i\theta}$.

$$V_{i\theta} = \frac{(\nu+\alpha)}{2}\frac{\partial}{\partial x_k}\left[f_{Vw}\frac{\partial \overline{u_i\theta}}{\partial x_k}\right] \quad (47)$$

$$\varepsilon_{i\theta} = C_\varepsilon f_{\varepsilon 1} f_{\varepsilon 2} f_{\varepsilon w}\frac{1+Pr}{2\sqrt{(Pr)}\sqrt{(R)}}\frac{\varepsilon}{k}\overline{u_i\theta}. \quad (48)$$

In the present study, $f_{\varepsilon w}$ and f_{Vw} are given in a simple form as:

$$f_{\varepsilon w} = f_{Vw} = \min\left[1, \frac{C_R}{R}+C_S\sqrt{(Re_t)}\right] \quad (49)$$

where the constant C_S is given a value of 0.1. Note that this modification only works for high Prandtl number flows, and it is not necessary for other cases (e.g., $Pr < O(10^1)$).

It is also important to satisfy the wall limiting behavior [29]. The terms that balance at the lowest order of y at the wall are $V_{i\theta}$, $\Pi_{i\theta}$ and $\varepsilon_{i\theta}$, and each of them requires some additional modification. In this study, the models proposed in the previous section are bridged with the expressions that satisfy the wall limiting behavior:

$$V_{i\theta} = \frac{\partial}{\partial x_k}\left[\left\{\frac{(\nu+\alpha)}{2}\frac{\partial \overline{u_i\theta}}{\partial x_k} + n_i n_j \frac{(\nu-\alpha)}{6}\frac{\partial \overline{u_j\theta}}{\partial x_k}\right\}f_w + \left\{\frac{(\nu+\alpha)}{2}\frac{\partial \overline{u_i\theta}}{\partial x_k}\right\}(1-f_w)\right] \quad (50)$$

$$\Pi_{i\theta} = -\frac{\varepsilon}{k}\overline{u_k\theta}n_k n_i f_w + C_\Pi f_{\Pi 1} f_{\Pi 2} C_P\sqrt{(Re_t)}\sqrt{\left(\frac{k}{2\overline{u^2_{(i)}}}\right)}\frac{\varepsilon}{k}\overline{u_i\theta} \quad (51)$$

$$\varepsilon_{i\theta} = \left\{\frac{1+Pr}{2Pr}\frac{\varepsilon}{k}\overline{u_i\theta} + \frac{1+Pr}{2Pr}\frac{\varepsilon}{k}\overline{u_k\theta}n_i n_k\right\}f_w + \left\{C_\varepsilon f_{\varepsilon 1} f_{\varepsilon 2}\frac{1+Pr}{2\sqrt{(Pr)}\sqrt{(R)}}\frac{\varepsilon}{k}\overline{u_i\theta}\right\}(1-f_w) \quad (52)$$

where n_i is the wall normal unit vector and f_w is a function that changes from unity to zero as it moves away from the wall. Note that only Model 1 of $\Pi_{i\theta}$ is used here since it can reproduce large anisotropy of scalar fluxes without any *ad hoc* wall reflection modeling. Although its form violates vectorial invariance, Model 1 shows great improvement in strongly sheared turbulence where the turbulence anisotropy is very large, if a coordinate axis is set parallel to the mean flow direction. Its simplicity is so attractive that it is adopted as the $\Pi_{i\theta}$ model for wall flows in this study. The function f_w is chosen as follows:

$$f_w = \exp[-C_{w1}\sqrt{(A)}] \quad (53)$$

where $C_{w1} = \max[4, 0.6Pr^{3/4}]$.

Referring to Kawamura and Hada [30], the $\tilde{\varepsilon}_\theta\,(=\varepsilon_\theta - 2\alpha(max[\partial\sqrt{(k_\theta)}/\partial y, 0])^2)$ equation is solved instead of ε_θ equation for the sake of numerical stability:

$$\frac{D\tilde{\varepsilon}_\theta}{Dt} = \alpha\frac{\partial^2\tilde{\varepsilon}_\theta}{\partial x_i^2} + \frac{\partial}{\partial x_k}\left(C_{\theta 3} f_R \frac{k}{\varepsilon}\overline{u_j u_k}\frac{\partial\tilde{\varepsilon}_\theta}{\partial x_j}\right) + C_{P1}\frac{P_\theta}{k_\theta}\tilde{\varepsilon}_\theta + C_{P2}\frac{P}{k}\tilde{\varepsilon}_\theta - C_{D1}\frac{\tilde{\varepsilon}_\theta}{k_\theta}\tilde{\varepsilon}_\theta - C_{D2}\frac{\tilde{\varepsilon}}{k}\tilde{\varepsilon}_\theta + E - \frac{\tilde{\varepsilon}_\theta\hat{\varepsilon}_\theta}{k_\theta} \quad (54)$$

where $\tilde{\varepsilon} = \varepsilon - 2\nu(\partial\sqrt{(k)}/\partial y)^2$, $\hat{\varepsilon}_\theta = 2\alpha(\partial\sqrt{(k_\theta)}/\partial y)^2$, $E = 2\alpha C_{w2}(k_\theta/\varepsilon_\theta)\nu^2(\partial^2\Theta/\partial y^2)^2$ and $C_{w2} = \max\ [0.1, 0.35-0.21Pr]$†.

Then the model is applied to fully developed turbulent channel flows. The DNS data of Kasagi *et al.* [32], Kasagi and Ohtsubo [33] and Kim and Moin

† The authors apologize for typos in the definitions of E and C_{w2} in the previous paper presented at the 9th Symposium of Turbulent Shear Flows [31].

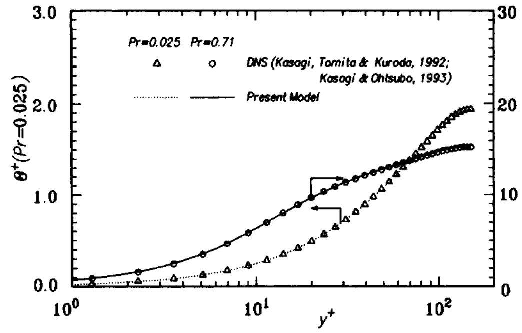

Fig. 6. Mean scalar profiles in fully developed turbulent channel flow.

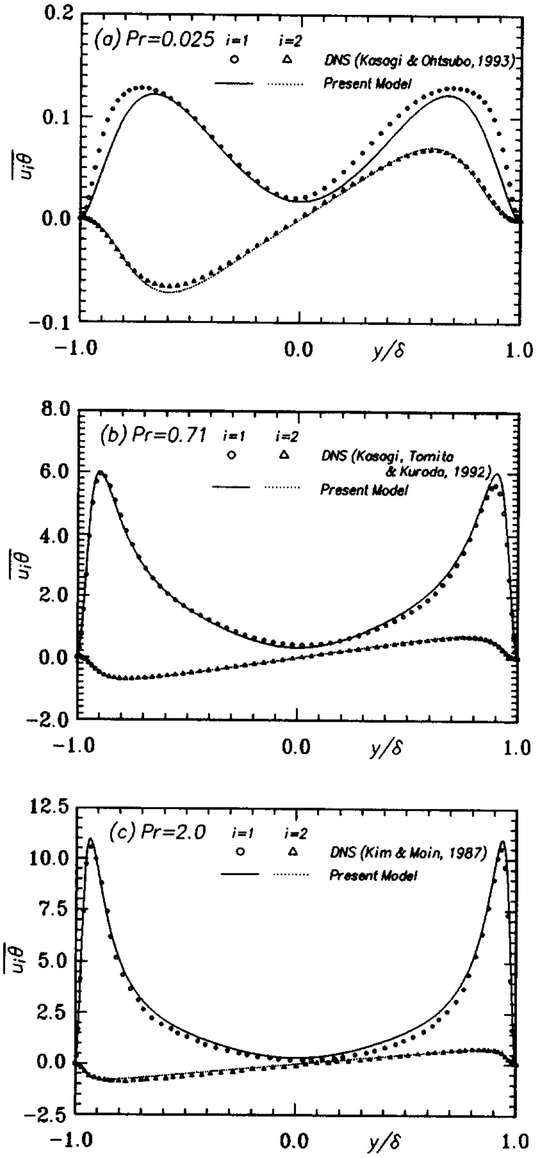

Fig. 7. Turbulent scalar flux profile in fully developed turbulent channel flow. (a) $Pr = 0.025$, (b) $Pr = 0.71$, (c) $Pr = 2.0$.

[34] are used. The mean scalar profiles at $Pr = 0.025$ and 0.71 are shown in Fig. 6. It can be said that the mean scalar profiles are well predicted in both cases. In Fig. 7, comparison is made with the DNS data at three different Prandtl numbers, i.e. $Pr = 0.025$, 0.71 and 2.0. The ratio of the two components of the scalar flux $-\overline{u_1\theta}/\overline{u_2\theta}$ changes drastically with increasing the Prandtl number; it becomes greater than 10 near the wall at $Pr = 2.0$. The present model captures even quantitatively well this strongly anisotropic feature of the scalar field. It is surprising that these results have been obtained with a simple $\Pi_{i\theta}$ model in which no wall reflection effect is taken into account. The predicted budget profiles of $\overline{u_2\theta}$ are compared with the DNS data in Fig. 8. In the budget of $Pr = 0.025$, the scalar-pressure gradient correlation term does not make any appreciable contribution and the dissipation balances with the production. For $Pr = 0.71$, however, the scalar–pressure gradient correlation term almost balances with the production term. This tendency is successfully predicted by the present model.

Finally, the Nusselt number Nu is plotted against a wide range of Prandtl number ($2.5\times10^{-2} < Pr < 10^4$) for $Re_\tau = 150$ in Fig. 9. The empirical function of Sleicher and Rouse [35] for pipe flows is also plotted for comparison. It is known that the Nusselt number is nearly proportional to $Pr^{1/3}$ at high Prandtl numbers, and this Prandtl number dependence is well predicted.

4. CONCLUSIONS

A second-moment closure is proposed for predicting turbulent scalar transport in various Prandtl number fluids. The correlation coefficients of the scalar–pressure gradient correlation and also of the dissipation terms are defined in the turbulent scalar flux equation. It is argued that these coefficients must decrease when the fluctuations arise at different scales and that the rate of decrease is to be proportional to the ratios between time scales and Taylor microscales involved. As a result, the present model coefficients are expressed as functions of the turbulent Reynolds number Re_t, the Prandtl number Pr and the time scale ratio R.

The present model predicts well the turbulent scalar fluxes in isotropic turbulence with a constant mean scalar gradient, where the model constants show large variations over wide Pr and Re_t ranges. The scalar–pressure gradient model, especially Model 1 given by equation (11), predicts well the large anisotropy of turbulent scalar flux in wall turbulence. Although Model 1 does not assume vectorial invariance, it shows great improvement in simple shear flows provided that one of the coordinate axis is defined in alignment with the main flow direction. Model 1 must be used with care in this respect.

Acknowledgements—The authors acknowledge the financial

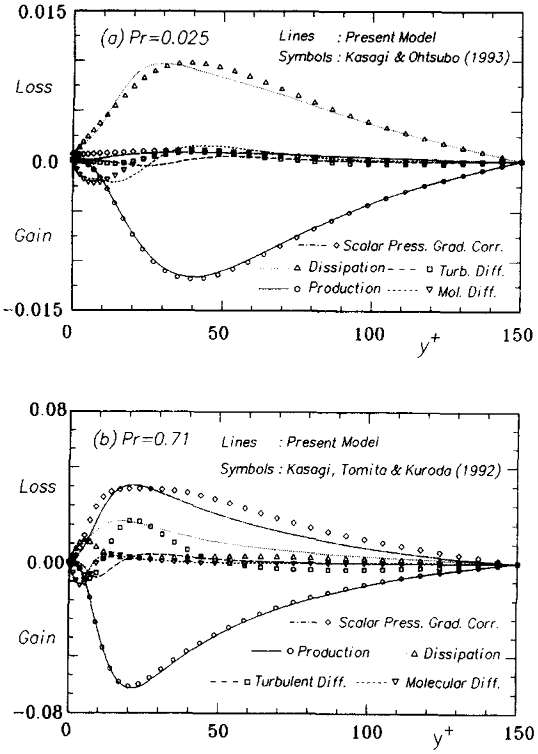

Fig. 8. Budgets of $\overline{u_2\theta}$ in fully developed turbulent channel flow. (a) Pr = 0.025, (b) Pr = 0.71.

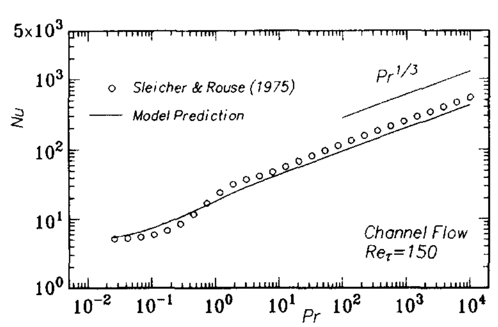

Fig. 9. Prandtl number dependence of Nusselt number in fully developed turbulent channel flow.

support through the Grant-in-Aids for Priority Area (No. 05240103) and for Encouragement of Young Scientists (No. 03003924) by the Ministry of Education, Science and Culture.

REFERENCES

1. M. M. Rogers, The structure of a passive scalar field with a uniform mean gradient in rapidly sheared homogeneous turbulent flow, *Phys. Fluids* **A3,** 144–154 (1991).
2. J. L. Lumley, Computational modeling of turbulent flows, *Adv. Appl. Mech.* **18,** 123–176 (1978).
3. C. G. Speziale, Turbulence modeling in noninertial frames of reference, *Theoret. Comput. Fluid Dynam.* **1,** 3–19 (1989).
4. T.-H. Shih and J. L. Lumley, Modeling of pressure correlation terms in Reynolds stress and scalar flux equations, Rep. FDA-85-3, Sibley School of Mechanical and Aerospace Engineering, Cornell University (1985).
5. T. J. Craft, Computational modelling of turbulent scalar transport, Report TFD/91/3, Mechanical Engineering Department, UMIST (1991).
6. F. S. Lien and M. A. Leschziner, Modelling 2D and 3D separation from curved surfaces with variants of second-moment closure combined with low-Re near-wall formulations, *Proceedings of the 9th Symposium on Turbulent Shear Flows* **2,** 13-1 (1993).
7. S. Murakami, A. Mochida and R. Ooka, Numerical simulation of flow field over surface-mounted cube with various second-moment closure models, *Proceedings of the 9th Symposium on Turbulent Shear Flows* **2,** 13-5 (1993).
8. C. G. Speziale, S. Sarkar and T. B. Gatski, Modelling the pressure-strain correlation of turbulence: an invariant dynamical systems approach, *J. Fluid Mech.* **227,** 245–272 (1991).
9. A. J. Reynolds, The prediction of turbulent Prandtl and Schmidt numbers, *Int. J. Heat Mass Transfer* **18,** 1055–1069 (1975).
10. M. Jischa and H. B. Rieke, About the predictions of turbulent Prandtl and Schmidt numbers from modeled transport equations, *Int. J. Heat Mass Transfer* **22,** 1547–1555 (1979).
11. H. K. Myong and N. Kasagi, Numerical prediction of turbulent pipe flow heat transfer for various Prandtl number fluids with the improved k–ε turbulence model, *JSME Int. J., Ser. II* **32,** 613–622 (1989).
12. Y. Nagano and C. Kim, A two equation model for heat transport in wall turbulent shear flows, *ASME J. Heat Transfer* **110,** 583–589 (1988).
13. K. Suzuki, An approach to liquid metal turbulent heat transfer in a circular tube solving $\overline{v\theta}$ equation with local equilibrium assumption, *Lett. Heat Mass Transfer* **9,** 245–254 (1982).
14. B. A. Kolovandin, Modeling the dynamics of turbulent transport processes, *Adv. Heat Transfer* **21,** 185–237 (1991).
15. W. P. Jones and P. Musonge, Closure of the Reynolds stress and scalar flux equations, *Phys. Fluids* **31,** 3589–3604 (1988).
16. H. Tennekes and J. L. Lumley, *A First Course in Turbulence*. MIT Press, Cambridge, MA (1972).
17. B. E. Launder, Second-moment closure: methodology and practice. In *Turbulence Models and Their Applications*, Vol. 2. Eyrolles (1984).
18. T.-H. Shih and A. Shabbir, Advances in modeling the pressure correlation terms in the second moment equations. In *Studies in Turbulence* (Edited by Gatski *et al.*) pp. 91–128. Springer, Berlin (1992).
19. S. B. Pope, Consistent modelling of scalars in turbulent flows, *Phys. Fluids* **26,** 404–408 (1983).
20. A. Matsumoto, Y. Nagano and T. Tsuji, Direct numerical simulation of homogeneous turbulent shear flow (in Japanese), *Proceedings of the 5th Symposium Comparative Fluid Dynamics*, pp. 361–363 (1991).
21. T.-H. Shih, J. L. Lumley and J.-Y. Chen, Second-order modeling of a passive scalar in a turbulent shear flow, *AIAA Jl* **28,** 610–617 (1990).
22. O. Iida, Private communication (1992).
23. O. Iida and N. Kasagi, Direct numerical simulation of homogeneous isotropic turbulence with heat transport: Prandtl number effects, (in Japanese), *Trans Jpn Soc. Mech. Engng* **59**(567), 3359–3364 (1993).
24. H. Maekawa and M. Kobayashi, (in Japanese), *Trans Jpn Soc. Mech. Engng* **43**(370), 2250–2260 (1977).
25. A. Sirivat and Z. Warhaft, The effect of a passive cross-stream temperature gradient on the evolution of temperature variance and heat flux in grid turbulence, *J. Fluid Mech.* **162,** 323–346 (1983).
26. S. Tavoularis and S. Corrsin, Experiments in nearly homogeneous turbulent shear flow with a uniform mean temperature gradient—1, *J. Fluid Mech.* **104,** 311–347 (1981).

27. M. M. Rogers, P. Moin and W. C. Reynolds, The structure and modeling of the hydrodynamic and passive scalar fields in homogeneous turbulent shear flow, Report TF-25, Department of Mechanical Engineering, Stanford University (1986).
28. N. Kasagi, A. Kuroda and M. Hirata, Numerical investigation of near-wall turbulent heat transfer taking into account the unsteady heat conduction in the solid wall, *ASME J. Heat Transfer* **111,** 385–392 (1989).
29. Y. G. Lai and R. M. C. So, Near-wall modeling of turbulent heat fluxes, *Int. J. Heat Mass Transfer* **33,** 1429–1440 (1990).
30. H. Kawamura and K. Hada, An evaluation of k–$\tilde{\varepsilon}$ model of wall turbulence, (in Japanese), *Proceedings of the 29th National Heat Transfer Symposium of Japan*, 380–382 (1992).
31. N. Shikazono and N. Kasagi, Modeling Prandtl number influence on scalar transport in isotropic and sheared turbulence, *Proceedings of the 9th Symposium on Turbulent Shear Flows* **2,** 18-3 (1993).
32. N. Kasagi, Y. Tomita and A. Kuroda, Direct numerical simulation of the passive scalar field in a turbulent channel flow, *ASME J. Heat Transfer* **114,** 598–606 (1992).
33. N. Kasagi and Y. Ohtsubo, Direct numerical simulation of low Prandtl number thermal field in a turbulent channel flow, *Turbulent Shear Flows* **8,** 97–119. Springer (1993).
34. J. Kim and P. Moin, Transport of passive scalars in a turbulent channel flow, *Proceedings of the 6th Symposium on Turbulent Shear Flows*, 5-2 (1987).
35. C. A. Sleicher and M. W. Rouse, A convenient correlation for heat transfer to constant and variable property fluids in turbulent pipe flow, *Int. J. Heat Mass Transfer* **18,** 677–683 (1975).